

Future millimeter, submillimeter and far-infrared surveys and their successful follow up

A. W. Blain

Institute of Astronomy, Madingley Road, Cambridge, CB3 0HA, UK

Abstract. The first unbiased surveys for high-redshift galaxies in the submillimeter (submm) and far-infrared (FIR) wavebands have been made over the last two years. When combined with the intensity of extragalactic background radiation in the same wavebands, we have a reasonable first view of the dust enshrouded Universe. Limited spatial resolution hampers the identification of the submm galaxies, and follow-up observations currently consume much larger amounts of telescope time than the initial submm-wave detections. Here the prospects for future submm/FIR surveys are discussed, highlighting the importance of planning careful multiwaveband radio/submm/FIR observations. These can be used to yield photometric redshift information. Radio observations are vital to give accurate positions for the detected sources.

1. Introduction

The history of dust obscured energy production in galaxies, whether due either to star-formation activity or to accretion onto active galactic nuclei (AGN), has been investigated (Guiderdoni et al. 1998; Blain et al. 1999a,c; Tan et al. 1999; Trentham et al. 1999), using data from a combination of surveys for high-redshift galaxies at $850\ \mu\text{m}$ using the SCUBA camera (Holland et al. 1999) (Smail et al. 1997; Barger et al. 1998; Hughes et al. 1998; Barger et al. 1999a; Blain et al. 1999b; Eales et al. 1999) and the determination of the submm/far-infrared (FIR) extragalactic background radiation intensity (Puget et al. 1996; Fixsen et al. 1998; Hauser et al. 1998; Schlegel et al. 1998). The bulk of the mm/submm-wave background radiation intensity at wavelengths longer than $500\ \mu\text{m}$ has now been resolved into discrete sources (Blain et al. 1999c). Existing measurements of the counts and background radiation intensity contributed by distant dusty galaxies are shown in Figs 1 & 2. In Fig. 1 counts derived using a well-constrained model (Blain et al. 1999b) are also shown. The confusion noise expected in surveys from dusty galaxies (Blain et al. 1998a,b), radio galaxies (Toffolatti et al. 1998) and the ISM (Helou & Beichman 1990) are shown in Fig. 3.

However, less than 100 submm-selected galaxies are currently known, and redshifts and high-quality multiwaveband data available for very few. The confirmation of their optical counterparts is currently a very time consuming process. First, an extremely deep VLA radio image is desirable, to give a sub-arcsec position for the submm galaxy. An optical redshift must then be found (e.g. Ivison et al. 1998), before a mm-wave interferometric detection of CO molecular line

emission at the same redshift confirms the identification unequivocally (Frayer et al. 1998, 1999). The observing time involved in this identification process is up to ten times greater than that required to detect each submm-luminous galaxy. In future mm/submm-wave surveys, using for example the wide-field BOLOCAM bolometer array camera (Glenn et al. 1998), the detection rate of galaxies should increase from a few per night to several per hour. Hence, even with access to the very finest facilities, this follow-up procedure will be completely inadequate to keep up with the growing catalog of submm galaxies.

Here we discuss how observations of dusty galaxies using future facilities over the next few years – in particular BOLOCAM, the long-wavelength MIPS instrument on *SIRTF* and the upgraded VLA – can be combined to provide redshift information without recourse to optical telescopes. Despite the large detection rate, the classification and identification of the most interesting detected galaxies for detailed follow-up observations should be able to keep pace.

2. The properties of luminous high-redshift dusty galaxies

Three galaxies detected in submm surveys have sure identifications, as well as two cD galaxies detected in clusters (Edge et al. 1999). These are ultraluminous galaxies at redshifts $z = 1.06, 2.56$ and 2.81 (Soucail et al. 1999; Frayer et al. 1998, 1999; Ivison et al. 1998, 2000). An important goal is to extend the size of the sample of submm-selected galaxies, and to identify a larger number. A wide range of powerful mm, submm and FIR instruments that are suitable for carrying out surveys (see Table 1) will become available over the next decade. Some of their specifications are listed in Table 1, along with the rate at which these instruments should be able to survey the sky and the depth at which they are expected to be affected by confusion noise. In Fig. 4 the detection rate of galaxies that could be achieved using these instruments are shown.

Note that while the Atacama Large Millimeter Array (ALMA) is a very powerful survey instrument, it will be most important for making resolved images of the galaxies detected using all the other facilities. The *Planck Surveyor* microwave background imaging satellite will also provide a very valuable all-sky survey at wavelengths between 10 mm and $350 \mu\text{m}$.

Detection rates of order 100 hr^{-1} are expected in future mm/submm-wave surveys, probing galaxies at $z > 1$, as compared with the current rate of about 0.2 hr^{-1} . Is it possible to make multiwaveband mm/submm/FIR observations using a combination of the instruments listed in Table 1, and to generate photometric redshifts for the detected sources?

3. Prospects for submm/FIR photometric redshifts

A common broad-band spectral energy distribution (SED) can describe most submm-selected galaxies: see Fig. 1 in Blain (1999; this volume). There are several possible ways to derive photometric redshifts from radio, mm, submm and FIR photometry assuming this SED, which has a very generic form at wavelengths longer than about $60 \mu\text{m}$.

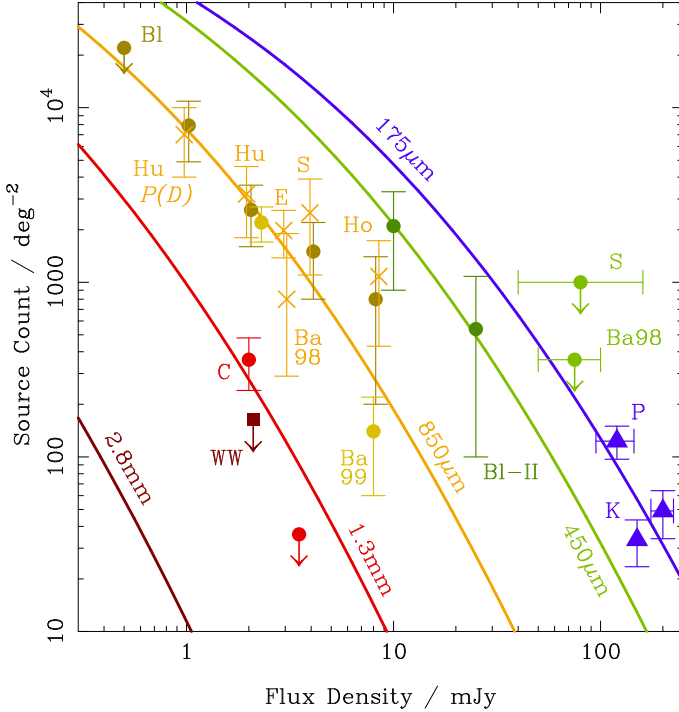


Figure 1. Counts of mm, submm and FIR galaxies. Data: Blain et al. (1999b, 2000) – Bl, Bl-II; Hughes et al. (1998) – Hu; Eales et al. (1999) – E; Smail et al. (1997) – S; Barger et al. (1999a) – Ba99; Barger et al. (1998) – Ba98; Holland et al. (1998) – Ho; Carilli et al. (2000) – C; Wilner & Wright (1997) – WW; Puget et al. (1999) – P; and Kawara et al. (1998) – K. The results at 2.8 mm (WW) are from BIMA, at 1.3 mm from IRAM, at 850 and 450 μm from SCUBA and at 175 μm from *ISO*. The lines are taken from the ‘modified gaussian model’, a modified version of the Blain et al. (1999b) ‘Gaussian model’, which accounts for the preliminary redshift distribution of SCUBA galaxies (Barger et al. 1999b).

1. The radio–submm spectral index. As discussed by Carilli & Yun (1999; 2000) and Blain (1999; this volume), the spectral break between non-thermal synchrotron emission and thermal dust emission, which typically occurs at a restframe wavelength of about 3 mm, can be used to provide redshift information. The quantity $(1+z)/T$, where T is the dust temperature can be determined reasonably accurately using this method: see Smail et al. (1999) for an application.
2. The position of the peak of the dust SED. Measurements at wavelengths on both sides of the redshifted peak of the dust SED can be used to fix the quantity $(1+z)/T$. This requires joint submm and FIR observations. See also Hines (1999; this volume).

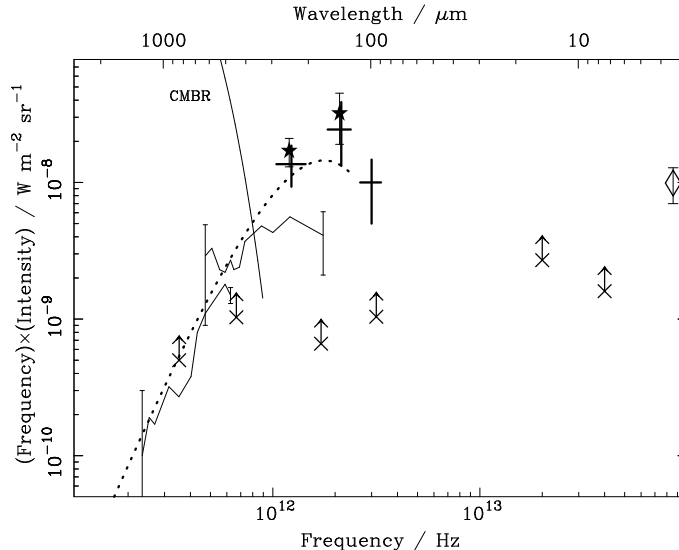


Figure 2. The background radiation intensity from the mm to near-IR wavebands. Solid line – Puget et al. (1996). Dotted line – Fixsen et al. (1998). Diagonal crosses (from left to right) – Blain et al. (1999b, 2000); Ivison et al. (1998, 2000); Kawara et al. (1998) and Puget et al. (1999); and (last pair) Altieri et al. (1999). Stars – Schlegel et al. (1998). Vertical crosses – Hauser et al. (1998) and Dwek et al. (1998). Diamond – Dwek & Arendt (1998).

3. The submm–optical flux density ratio. Distant dusty galaxies seem to show a wide range of optical properties (Smail et al. 1998; Barger et al. 1999b; Ivison et al. 2000), but more distant galaxies should typically be optically fainter, because of the very different K -corrections in each band. This information could be used to provide a coarse indication of redshift.
4. Mid-IR (MIR) and near-IR spectral features can be exploited to provide redshift information. This is outside the scope of this paper: see Xu et al. (1998) and Simpson & Eisenhardt (1999) for more information.

The issue of cross identification between surveys at different wavelengths should not be too challenging. At the relevant wavelengths of 1.1 mm (CSO-BOLOCAM) and 160, 70 and 24 μm (*SIRTF*-MIPS), the angular resolution of the survey maps will be well matched, at about 30, 45, 20 and 7 arcsec respectively. The sub-arcsec positional accuracy of a VLA detection will allow a counterpart source to be sought in deep optical and near-IR images.

4. The best prospects for future surveys

New instruments that will be coming into service over the next few years are listed in Table 1. Of these the most timely and powerful are BOLOCAM, *SIRTF* and the upgraded VLA, which will cover the MIR/FIR, mm and radio wavebands. However, the disparate mapping speeds of each instrument mean that

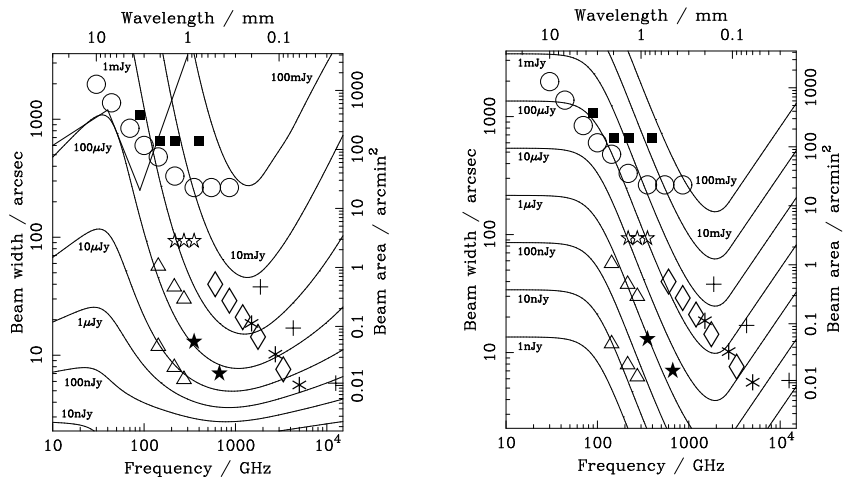


Figure 3. $1\text{-}\sigma$ confusion noise expected in mm to FIR surveys. Left: due to dusty external galaxies (extended from Blain et al. 1998a,b). Radio-loud objects may make a significant contribution to the top left of the jagged solid line (Toffolatti et al. 1998). Right: due to the Milky Way ISM, if the surface brightness $B_0 = 1 \text{ MJy sr}^{-1}$ at $100 \mu\text{m}$: see Helou & Beichman (1990), and data from Gautier et al. (1992), Désert et al. (1990) and Finkbeiner et al. (1999). The ISM confusion noise scales as $B_0^{1.5}$. The extrapolations to arcsecond scales are potentially uncertain. Experiments are shown by: circles – *Planck Surveyor*; squares – BOOMERANG; empty stars – SuZIE; triangles – BOLOCAM (CSO above; LMT below); filled stars – SCUBA; diamonds – *FIRST*; asterisks – SOFIA; crosses – *SIRTF*. ALMA and *SPECS* have resolution limits below the bottom of the frames.

different combinations of overlapping surveys will be required. To best exploit the capabilities of *SIRTF* and BOLOCAM, there seem to be three clear survey strategies. The photometric redshift information that can be derived from each survey is shown in the 3 panels of Fig. 5.

1. A 1.1-mm BOLOCAM survey at the 10-m CSO mapping at the most efficient depth, $5\text{-}\sigma \simeq 10 \text{ mJy}$ (Fig. 4). About 4 galaxies per hour should be detected, and ultimately about 50 hr^{-1} at the 50-m LMT. These mm-wave surveys will be a very efficient way to detect high-redshift galaxies; almost all of the detected sources should be at $z > 1$, about 50% at $z > 2$, and about 10% at $z > 5$ (Barger et al. 1999a; Blain et al. 1999c).
2. A $160\text{-}\mu\text{m}$ *SIRTF* survey to an efficient detection depth of 100 mJy (Fig. 4), surveying about 3 deg^2 per hour and detecting about 300 galaxies per hour. This survey exploits *SIRTF*'s longest wavelength band to boost the number of high-redshift galaxies detected; 80% of the detected sources are expected to be at $z > 1$, and about 10% at $z > 2$.

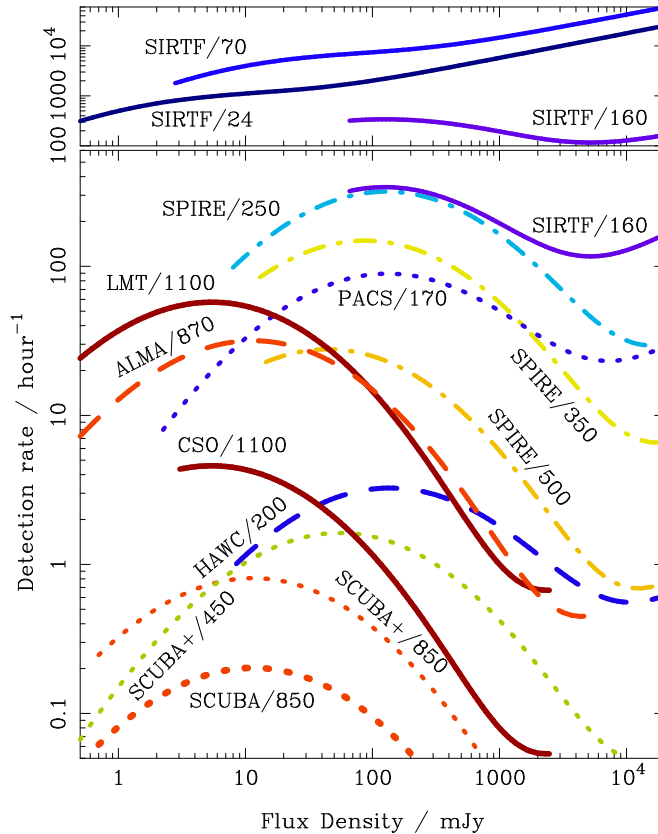


Figure 4. The detection rate as a function of $5\text{-}\sigma$ depth in a range of surveys. Numbers are the observing wavelengths in μm . HAWC is the FIR camera for SOFIA; SPIRE (PACS) is the long-(short-)wave imaging instrument for *FIRST*; BOLOCAM will operate at the CSO and the 50-m LMT. The curves stop at about the confusion limit (left) and where the count falls below $1/4\pi \text{ sr}^{-1}$ (right).

3. A $70\text{-}\mu\text{m}$ *SIRTTF* survey to a confusion limited depth of 3 mJy . This will yield a tremendously large number of sources, at a rate of about 6000 hr^{-1} . A shallower wider survey in this band would lead to an even greater detection rate: see Fig. 4. About 60% of the detected galaxies are expected to be at $z > 0.5$, and about 5% at $z > 2$.

4.1. Following up and finding photometric redshifts

By making coupled FIR/MIR *SIRTTF* observations of CSO-BOLOCAM survey fields, the form of the SED of the detected galaxies will be constrained. At 160 and $70 \mu\text{m}$, about 9 and 23% of the time spent surveying at 1.1-mm is required to reach the confusion limits of 70 and 6 mJy respectively at $5\text{-}\sigma$ significance. At 1.4 GHz , $24 \mu\text{m}$ and $8 \mu\text{m}$, using the upgraded VLA, MIPS and IRAC respectively, 10% of the 1.1-mm integration time will yield deep, unconfused maps to a $5\text{-}\sigma$ depth of $70 \mu\text{Jy}$, 2 mJy and 0.15 mJy respectively. At the top of Fig. 5 the efficiency of combining all this data to generate photometric redshifts can be

seen. The radio–submm flux density ratio will typically provide useful information on the value of $X = (1+z)(T/40\text{ K})^{-1}$ if $X < 3$, while the *SIRTF*-MIPS data is useful to $X < 4$. Note that the sources detected will be several times brighter than the existing SCUBA galaxies. Deep ALMA high-resolution imaging of sources not detected in the initial VLA survey can be carried out in 1-min integration.

Observations with the upgraded VLA can cover the field of a 160- μm *SIRTF* survey to a 5σ sensitivity of $120\ \mu\text{Jy}$ in 100% of the time allocated to *SIRTF*. At this sensitivity, detections should be obtained for all values of X (see the middle of Fig. 5); however, the shallow slope of the radio–FIR flux density ratio means that the photometric redshift information derived will be relatively noisy. From Fig. 5, 5σ sensitivities of about 20 and 3 mJy are required to detect a 100-mJy 160- μm source for interesting values of X . Maps to this sensitivity can be obtained in the 70- and 24- μm MIPS channels in 100% of the time allocated to the 160- μm survey. mm-wave BOLOCAM observations cannot be made over the whole 160- μm *SIRTF* survey field to a depth sufficient to detect 160- μm sources at interesting flux densities in a reasonable time, even at the LMT.

Although the detection rate of galaxies in a 70- μm *SIRTF* survey will be very large, the survey will be impossible to follow-up in its entirety at other mm/FIR wavelengths until the arrival of the ALMA and *SPECS*. However, in a time-matched survey, the VLA could reach a 5σ depth of $4.7\ \mu\text{Jy}$, detecting and providing an accurate position for *SIRTF* 70- μm sources for all values of X (see bottom of Fig. 5). A LMT-BOLOCAM survey could cover the same area to a 5σ depth of 0.5 mJy in the same integration time, sufficient to provide redshift information if $X > 2.5$.

4.2. Other instruments

The ALMA has excellent sensitivity, and so follow-up imaging observations to resolve the detected sources will be very rapid (see Blain 2000). This will also be true for the *SPECS* space interferometer. The *SIRTF*-IRAC camera, operating at its longest wavelength of $8\ \mu\text{m}$ will also be a very powerful instrument for detecting distant galaxies. However, because the models here are tuned to make predictions at longer wavelengths, refer to Eisenhardt (1999; this volume) for predictions of the performance of IRAC.

5. Conclusions

The first generation of submm surveys have now resulted in significant understanding of dust obscuration in the high-redshift Universe, but only a few examples of well studied submm-selected star-forming galaxies and active galactic nuclei are known. Within the next few years BOLOCAM and *SIRTF* should dramatically increase the size of samples. By carefully combining the surveys made by these instruments and the upgraded VLA, photometric redshifts should be available for up to 90% of the detected galaxies, thus providing information with which to test models of galaxy evolution and to prioritize follow-up observations.

Acknowledgments. I thank Ian Smail, Rob Ivison and Jean-Paul Kneib for the success of the SCUBA lens survey and useful discussions. Also Lee

Armus, Jaime Bock, Len Cowie, Jackie Davidson, Eli Dwek, Peter Eisenhardt, Jason Glenn, Dean Hines, Andrew Lange, Dave Leisawitz and OCIW.

References

- Altieri, B., et al. 1999, *A&A*, 343, L65
Barger, A. J., et al. 1998, *Nature*, 394, 248
Barger, A. J., Cowie, L., & Sanders D. 1999a, *ApJ*, 518, L5
Barger, A. J., et al. 1999b, *AJ*, 117, 2656
Blain, A. W. 1999, this volume (astro-ph/9905248)
Blain, A. W. 2000, conference proceeding (astro-ph/9911449)
Blain, A. W., Ivison, R. J., & Smail, I. 1998a, *MNRAS*, 296, L29
Blain, A. W., et al. 1998b, conference proceeding (astro-ph/9806063)
Blain, A. W., Jameson, A. J., Smail, I., et al. 1999a, *MNRAS*, 309, 715
Blain, A. W., Kneib, J.-P., Ivison, R. J., & Smail, I. 1999b, *ApJ*, 512, L87
Blain, A. W., Smail, I., Ivison, R. J., & Kneib, J.-P. 1999c, *MNRAS*, 302, 632
Blain, A. W., Ivison, R. J., Kneib, J.-P. & Smail, I. 2000, (astro-ph/9908024)
Bock, J. J. 1999, private communication
Carilli, C. L., & Yun, M. S. 1999, *ApJ*, 513, L13
Carilli, C. L., Menten K. M., et al. 2000 (astro-ph/9907436)
Carilli, C. L., & Yun, M. S. 2000, *ApJ*, in press (astro-ph/9910316)
Davidson, J. A. 1999, *Ap&SS*, in press
Désert, F.-X., Boulanger, F., & Puget, J.-L., 1990, *A&A*, 237, 215
Dwek, E., & Arendt, R. 1998, *ApJ*, 508, L9
Dwek, E., et al. 1998, *ApJ*, 508, 106
Eales, S. A., et al. 1999, *ApJ*, 515, 518
Edge, A. C., et al. 1999, *MNRAS*, 306, 599
Eisenhardt, P. 1999, this volume
Finkbeiner, D., Davis, M., & Schlegel, D. 1999, *ApJ*, 524, 867
Fixsen, D. J., et al. 1998, *ApJ*, 508, 123
Frayser, D. T., et al. 1998, *ApJ*, 506, L7
Frayser, D. T., et al. 1999, *ApJ*, 514, L13
Gautier, T., et al. 1992, *AJ*, 103, 1313
Glenn, J., et al. 1998, *Proc. SPIE*, 3357, 326
Guiderdoni, B., Hivon, E., et al. 1998, *MNRAS*, 295, 877
Hauser, M. G., et al. 1998, *ApJ*, 508, 25
Helou, G., & Beichman, C. A. 1990, *ESA SP-314*, ESA: Paris, 117
Hines, D. 1999, this volume
Holland, W. S., et al. 1998, *Nature*, 392, 788
Holland, W. S., et al. 1999, *MNRAS*, 303, 659
Hughes, D., et al. 1998, *Nature*, 394, 241

Iverson, R. J., et al. 1998, MNRAS, 298, 583
Iverson, R. J., et al. 2000, MNRAS, in press (astro-ph/9911069)
Kawara, K., et al. 1998, A&A, 336, L9
Mather, J. C., et al. 1998, preprint (astro-ph/9812454)
Puget, J.-L., et al. 1996, A&A, 308, L5
Puget, J.-L., et al. 1999, A&A, in press (astro-ph/9812039)
Schlegel, D. J., Finkbeiner, D. P., & Davis, M. 1998, ApJ, 500, 525
Simpson, C., & Eisenhardt, P. 1999, PASP, 111, 691
Smail, I., Iverson, R. J., & Blain, A. W. 1997, ApJ, 490, L5
Smail, I., Iverson, R. J., Blain, A. W., & Kneib, J.-P. 1998, ApJ, 507, L21
Smail, I., Iverson, R. J., et al. 2000, ApJ, in press (astro-ph/199907083)
Soucail, G., et al. 1999, A&A, 343, L70
Tan, J. C., Silk, J., & Balland, C. 1999, ApJ, 522, 579
Toffolatti, L., et al. 1998, MNRAS, 297, 117
Trentham, N., Blain, A. W., & Goldader, J., 1999, MNRAS, 305, 61
Wilner, D. J., & Wright, M. C. H. 1997, ApJ, 488, L67
Xu, C., et al. 1998, ApJ, 508, 576

Table 1. Wavelengths λ , sensitivities (as noise equivalent flux density – NEFD), fields of view (FOV), mapping speeds and confusion limits due to galaxies and the ISM for future surveys. The speed presented is the mapping rate required to reach a $5\text{-}\sigma$ detection at a depth of 10 mJy, which depends on the square of the detection flux density limit. The confusion noise is defined as the flux at which there is one source per beam (see Fig. 3). The ISM confusion (in brackets) is calculated for a $100\text{-}\mu\text{m}$ surface brightness $B_0=1\text{ MJy sr}^{-1}$ and scales as $B_0^{1.5}$.

Name	λ (μm)	NEFD ($\text{mJy}/\sqrt{\text{Hz}}$)	FOV (arcmin^2)	Speed ($\text{deg}^2\text{ hr}^{-1}$)	Confusion (mJy)
SCUBA+	850	40	1.7	4.3×10^{-3}	0.12 (9×10^{-4})
	450	120	1.7	4.8×10^{-4}	0.053 (3×10^{-3})
SCUBA-II ⁱ	850	50	64	2.6	0.12 (9×10^{-4})
	450	200	64	0.16	0.053 (3×10^{-3})
SOFIA ^a	200	408	9.0	2.8×10^{-4}	1.2 (0.30)
BOLOCAM-CSO ^b	1100	42	44	0.10	0.32 (2×10^{-3})
BOLOCAM-LMT ^b	1100	2.8	2.5	1.6	6×10^{-3} (4×10^{-5})
<i>FIRST</i> -SPIRE ^c	500	114	40	1.2×10^{-2}	2.9 (0.16)
	350	90	40	2.0×10^{-2}	2.6 (0.12)
	250	84	40	2.3×10^{-2}	1.6 (0.24)
<i>FIRST</i> -PACS ^c	170	1.6	16	6.9×10^{-3}	0.45 (0.16)
	90	3.6	16	1.4×10^{-3}	0.01 (0.01)
<i>SIRTF</i> -MIPS ^d	160	18	2.5	3.1×10^{-2}	6.6 (3.1)
	70	4.5	25	5.0	0.28 (0.07)
	24	1.8	25	31	6×10^{-4} (2×10^{-4})
ALMA ^e	870	1.1	0.07	0.24	$< 10^{-7}$ ($< 10^{-6}$)
	450	15	0.02	3.7×10^{-4}	$< 10^{-8}$ ($< 10^{-4}$)
<i>SPECS</i> testbed ^f	250	0.17	4	0.46	$\sim 10^{-5}$ ($\sim 10^{-3}$)
<i>SIRTF</i> -IRAC ^d	8.0	0.15	25	0.44 (0.1 mJy)	$< 10^{-6}$ ($\sim 10^{-6}$)
	5.8	0.10	25	Simultaneous	Similar to above
	4.5	0.022	25	Simultaneous	Similar to above
	3.6	0.022	25	Simultaneous	Similar to above
Upgraded VLA	20.5 cm	0.40	700	2.0 (0.1 mJy)	... (...)

^aDavidson et al. (1999); <http://sofia.arc.nasa.gov/>

^bGlenn et al. (1998); <http://www-lmt.phast.umass.edu/ins/continuum/bolocam.html>

^cBock (1999)

^d<http://ssc.ipac.caltech.edu/sirtf/>

^e<http://www.alma.nrao.edu>

^fMather et al. (1998); <http://www.gsfc.nasa.gov/astro/specs/>

ⁱ<http://www.jach.hawaii.edu/JACpublic/JCMT/scuba/scuba2>

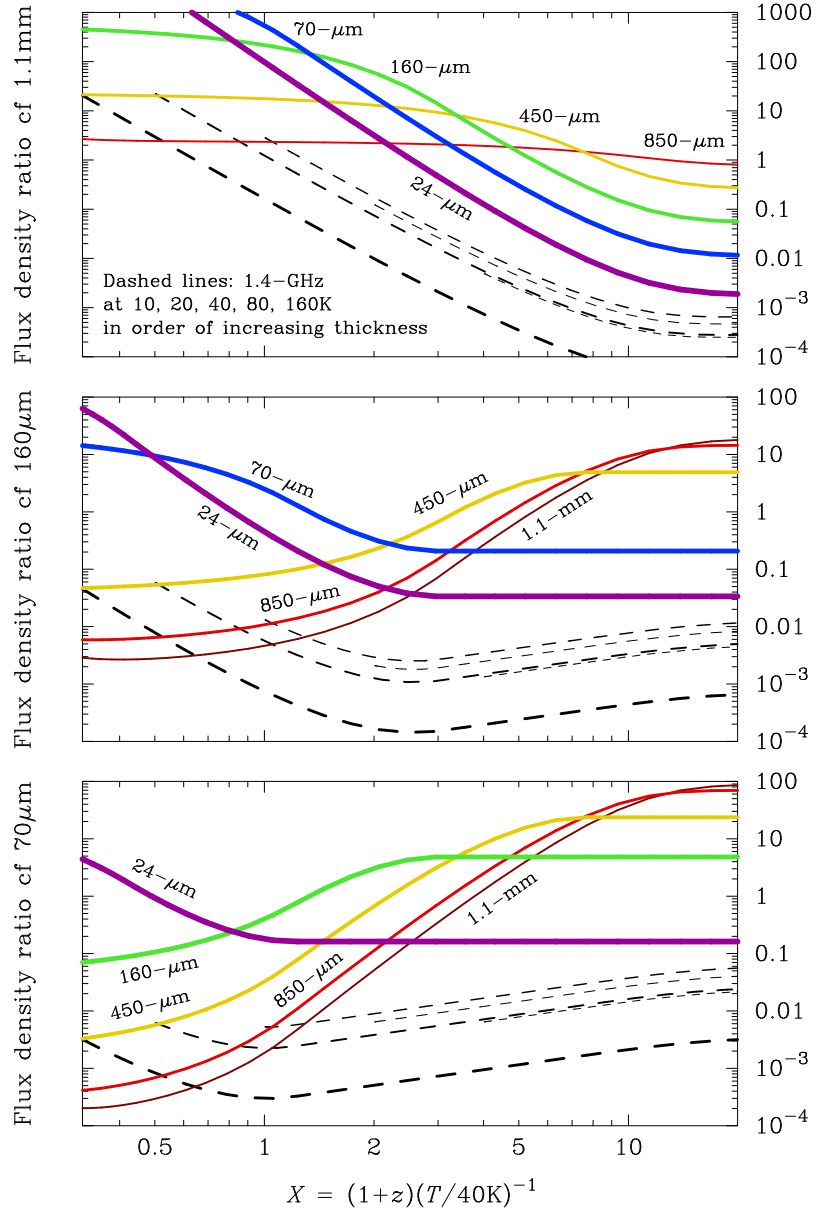


Figure 5. Flux density ratios expected at a range of wavelengths in the radio, mm, submm and FIR wavebands, as compared with survey wavelengths of 1.1 mm (top), 160 μm (middle) and 70 μm (bottom), appropriate to BOLOCAM and *SIRTF*-MIPS surveys. If the curves have a slope, rather than being horizontal, then the ratio is a potentially useful photometric redshift indicator, if the source is sufficiently bright to be detected in both bands. Note that little information is provided by a measurement in the 450/850- μm atmospheric windows unless $X > 5$. Hence, air-/space-borne observations at shorter wavelengths are required to constrain X over the likely range of redshifts for sources detected in a mm-wave survey.